© Universiti Tun Hussein Onn Malaysia Publisher's Office

IJIE

Journal homepage: http://penerbit.uthm.edu.my/ojs/index.php/ijie
ISSN : 2229-838X e-ISSN : 2600-7916

The International Journal of Integrated Engineering

Design and Simulation Study of Excitation Coil System with Different Array Configurations for Magnetic Particle Imaging Application

Muhd Fikri Shahkhirin Birahim[1], Nurmiza Othman[1,2*], Syarfa Zahirah Sapuan[1,2], Mohd Razali Md Tomari[1, 2]

[1]Faculty of Electrical and Electronic Engineering,
Universiti Tun Hussein Onn Malaysia, Batu Pahat, Johor, 86400, MALAYSIA

[2]Centre of Electromagnetic Compatibility (EMC),
Universiti Tun Hussein Onn Malaysia Batu Pahat, Johor, 86400, MALAYSIA

*Corresponding Author

DOI: https://doi.org/10.30880/ijie.2020.12.03.032
Received 18 December 2019; Accepted 14 January 2020; Available online 27 February 2020

Abstract: Magnetic Particle Imaging (MPI) is a tomographic imaging method has been introduced for three-dimensional (3D) imaging of human body with some potential applications such as magnetic hyperthermia and cancer imaging. It involves three important elements; tracer development using magnetic nanoparticles (MNPs), hardware realization (scanner using excitation and pickup coils), and image reconstruction optimization. Their combination will produce a high-quality image taken from any biological tissue in the human body based on the secondary magnetic field signal from the magnetized MNPs that are injected into human body. A homogeneous and adequate magnetic field strength from an excitation coil is needed to enhance the quality of the secondary signal. However, the complex surface topography of human body and physical properties of an excitation coil influence the strength and the homogeneity of the magnetic field generation at the MNPs. Therefore, this paper presents a new concept of excitation coil configuration to improve the magnetic field strength and the homogeneity to obtain better magnetization of MNPs to be detected in MPI. Two designs will be proposed with variation in physical properties and coil arrangement based on simulation study that will be carried out by using ANSYS Maxwell to generate magnetic field strength and homogeneity towards the targeted distance of 10 mm - 50 mm below the coils. The obtained magnetic field from the simulation was validated by the mathematical calculation using Biot-Savart Law equation. As a result, the new concept of excitation coil configuration proposed can be used to improve the MPI scanner system performance for various medical application.

Keywords: Magnetic Particle Imaging (MPI), Magnetic nanoparticles (MNPs), 3D analysis

1. Introduction

The Magnetic Particle Imaging (MPI) is a tracer-based tomographic imaging technique that can determine the three-dimensional (3D) distribution of the magnetic nanoparticles (MNPs) concentration. Although MPI is in the preclinical stage, there are still several features that are needed for future development such as high-resolution image contrast, signal-to-noise ratio (SNR), tracer's material, acquisition time for image reconstruction and coil design configuration [1]-[4] Over the last decades, Gleich and Weiznecker had invented MPI at Philips Research Laboratories in Hamburg, Germany. They had utilized the magnetization behaviour of the nanoparticle for tomographic imaging [5]. Since from the first

*Corresponding author: nurmiza@uthm.edu.my

invention of the MPI, many groups had explored and discovered the important features of the MPI, which are the material of the nanoparticle, magnetic coil design and image reconstruction technique. Previous studies have shown the rapid development of MPI. Until now, there is only one manufacturer which is Bruker that announces the world's first preclinical MPI system in 2013 [6]. A summary of the overall MPI development is listed in Table 1.

Table 1 - Summary of the overall MPI development

Year	Milestones
2005	Gleich and Weiznecker proposed the Magnetic Particle Imaging (MPI), a novel imaging method that has the ability of static imaging [5]
2007	Weizenecker et al. published a simulation study on the spatial resolution and sensitivity [7]
2008	Sattel et al. developed an alternative single-sided coil topology and showed dynamic 1D phantom images produced [8]
2009	Knopp et al. proved the theoretical foundations for a feasible coil topology for field-free line (FFL) imaging method [9]
2010	Knopp et al. introduced a model-based reconstruction of the MPI system [10]
2011	Knopp et al. analysed and derived simple resolution expression of the spatial resolution [11]
2013	The world's first preclinical MPI system was announced by Bruker [6]
2014	Vogel et al. developed the first hybrid MRI/MPI system [12]
2015	Zheng et al. developed the MPI system for stem cell imaging [13]
2016	Grafe et al. recorded 2D images with MPI scanner [14]
2017	Ohki et al. developed the MPI scanner system for hyperthermia [15]
2018	Muslu et al. proposed method to generate a multi-colour relaxation map in the MPI system [16]
2019	Kosch et al. developed solid phantoms containing freeze-dried MNPs for the comparison of resolution capabilities between different MPI scanners [17]

The basic concept of the MPI operation is started with the MNPs being injected into a subject [18]. The MNPs is made up of Superparamagnetic Iron Oxide Nanoparticle (SPION) that has a unique magnetization characteristic modelled by the Langevin theory [19]. Then, the MNPs accumulates in the targeted area to be detected by the receive coil after excited by the excitation field from the excitation coil. Lastly, the collected data from the receive coil will be used for the image reconstructed phase that indicates the locations and concentrations of the MNPs. There are three main components of the MPI scanner which are MNPs, magnetic coil (excitation coil, selection coil and receive coil) and image reconstruction. In this study, the effects of the excitation coil configuration have been investigated by different physical arrangement and parameter setting. The aim of this study was to generate a strong and homogeneous magnetic field from the excitation coil towards the MNPs at the targeted distance of 10 mm - 50 mm. (1 A) the current was supplied to the excitation coil to ensure the minimal power to be used in the whole magnetic field generation.

2. Materials and Methods

Two different types of coil configuration were designed and simulated, Design *A* and Design *B*. Then, both coil designs were determined with respect to their magnetic field strength and homogeneity towards the MNPs at the targeted distance by using ANSYS Maxwell simulation software. The magnetic field strength generated from the coil system was determined from 10 mm - 50 mm under the bottom surface of the coil as shown in Fig. 1. The difference between the two coil designs was the coil configurations arrangement to obtain a complete excitation coil system while the other specification parameters were set up to a similar value. The standard specification parameters were the amount of current supplied (1 A) to all coils for both coil designs, the material used for winding the coil (copper wire), coil shape (cylindrical), and the length of coils (50 mm). Since all the excitation coil proposed by previous researches used copper wire, therefore copper wire was chosen for both coil models [20]-[23]. The simulation results between both coil designs were compared in terms of the magnetic field strength and its homogeneity. Then, the simulation data obtained from the coil design that produces a better result was validated by the mathematical calculation based on the Biot-Savart Law.

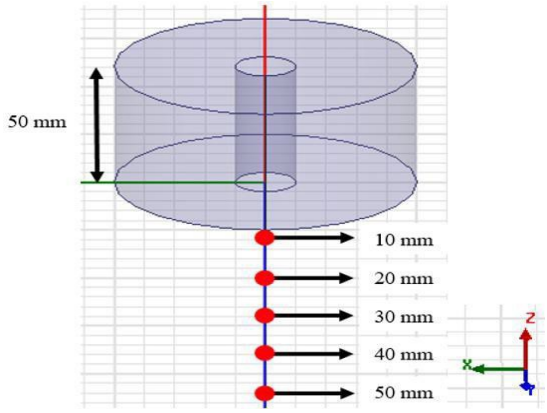

Fig. 1 - The magnetic field was determined from the distance of (10 mm - 50 mm) under the bottom surface of the coil

2.1 Design *A* Coil System

Design *A* coil system was designed with the specification as shown in Table 2. The arrangement of all coils to obtain the complete system as shown in Fig. 2. The length of all coils was 50 mm. The inner and outer radius of the one single-coil was 10 mm and 50 mm respectively as shown in Fig. 2 (a). The radius of a single wire was 1 mm and produce 2000 turns that winding one single coil. Copper wire was chosen to be used as coil wire and 1 A of current was supplied to all coils. The size of the distributed area to be measured was 120 mm × 100 mm in *xy*-plane (yellow plane) as shown in Fig. 2 (b).

Table 2 - Coil specification of Design *A*

Specification	Value
Length of the one single coil	50 mm
Inner radius, *a*	10 mm
Outer radius, *b*	50 mm
Wire radius	1 mm
Turns, *N*	2000
Wire material	Copper
Current, *I*	1A

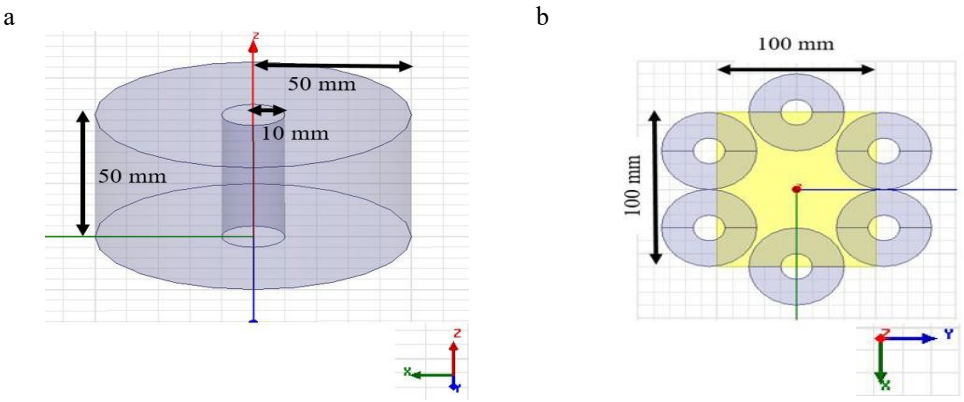

Fig. 2 - (a) one single coil of the Design *A* from *xyz*-axis view; (b) six coils used to obtain Design *A* coil system from the *xy*-axis view

2.2 Design *B* Coil System

Design *B* coil system was arranged with the specification as shown in Table 3. In this design, a Maxwell coils pair was employed together with other five single coils to obtain the complete excitation coil system. In MPI, Maxwell coils pair was used to create field-free-region (FFR) for MNPs magnetization purpose [24]. An example of a Maxwell coils pair configuration can be found in Fig. 3. Two identical circular coils are arranged symmetrically along the same axis. Each coil carries an equal amount of current, *I* flowing in the opposite direction. The blue coils indicate the Maxwell coils pair configuration and generated the field-free point (FFP) between the Maxwell coils pair.

In the Design *B*, five stacked coils (red coils) were arranged vertically between the Maxwell coils pair (blue coils) as can be found in Fig. 4 (a). The length of coil 1 and 2 (blue coils) was 50 mm for each coil while the length of coil 3, 4, 5, 6 and 7 (red coils) was 10 mm for each coil. The inner and outer radius of all coils was 10 mm and 50 mm respectively. The radius of the wire used was 1 mm for all coils. Copper wire was chosen to winding all coils and 1 A current was supplied to each of them. The size of the distributed area to be measured was 200 mm × 200 mm in *xy*-plane (yellow plane) as shown in Fig. 4 (b).

Table 3 - Coil specification of Design *B*

Specification	Value
Length of coil 1 & 2	50 mm
Length of coil 3, 4, 5, 6, & 7	10 mm
Inner radius, *a*	10 mm
Outer radius, *b*	50 mm
Wire radius	1 mm
Wire material	Copper
Current, *I*	1 A

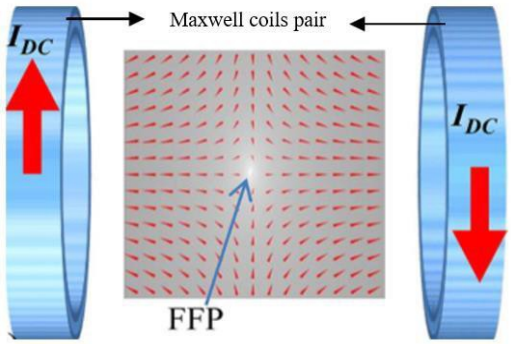

Fig. 3 - An example of the Maxwell coils pair in the conventional MPI system [24]

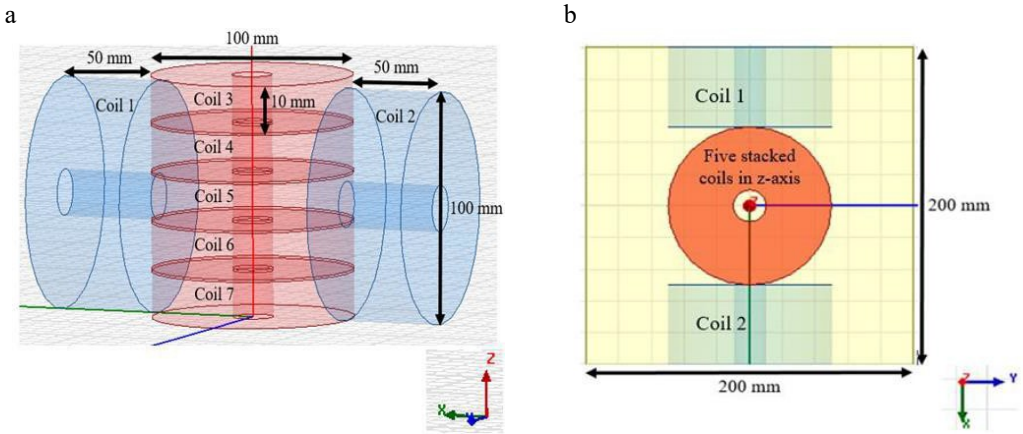

Fig. 4 - (a) Design *B* coils configuration from *xyz*-axis view; (b) Design *B* coils configuration from *xy*-axis view

2.3 Theoretical Calculation of Magnetic Field Strength Generated by the Coils

Based on the magnetic field strength generated by both coil designs, the better simulation data produced will be validated by the theoretical calculation work. The magnetic field strength generated by the coil design will be compared between the simulation data and calculation based on the extended equation of the Biot-Savart's Law as shown in equation (1) [23].

From equation (1), B indicates the magnetic field strength, μ_0 is the permeability in a vacuum (1.25664 x10−6), N is the number of turns, I is current, $2L$ is the length of the coil, a is the inner radius of the coil, b is the outer radius of coil and p is the vertical distance of the MNPs from the centre of the coil.

$$B = \frac{\mu_0 NI}{4(b-a)}\left[p \ln\left\{\frac{b+\sqrt{b^2+p^2}}{a+\sqrt{a^2+p^2}}\right\} - (p-2L)\ln\left\{\frac{b+\sqrt{b^2+(p-2L)^2}}{a+\sqrt{a^2+(p-2L)^2}}\right\}\right] \quad (1)$$

3. Results and Discussion

3.1 Magnetic Field Strength Generated from Both Coil Designs

Table 4 and Fig. 5 shows the comparison of the magnetic field strength generated from the Design *A* and Design *B* coil systems. From the simulation results, as shown in table 4 and Fig. 5, it can be seen that the magnetic field strength produced by the coils from the Design *B* was higher than the Design *A*. This is because the five vertically stacked coils arranged between the Maxwell coils pair in the Design *B* produced magnetic field in the same direction of z-axis and resulted in a higher total value of the magnetic field strength generated at the targeted distance of 10 mm - 50 mm below the surface of the most bottom coil in the design. Then, the magnetic field summation between each of the five vertically stacked coils can be calculated using the extended version of the Biot-Savart's Law equation as will be discussed in subsection 3.3.

Besides, the magnetic field strength generated from the coils was affected by the power loss to the surrounding. In order to generate high magnetic field strength, the power loss from the coils must be reduced and it can be done by decreasing the copper loss. Copper loss is the term given to heat produced by electrical currents in the winding conductors [25]-[27]. The power loss from the copper loss is given in equation (2) [28]. Where I is current, R is resistance and t is the time current is supplied. When the current was supplied to the coils, the copper loss will occur. The copper loss will increase when the resistance of the coil increase as long as the current supplied is maintained. The resistance of the coil was influenced by resistivity, length and area of the wire used as can be found in equation (3) [29]. Length of one single-coil from five stacked coils in Design *B* was shorter than in Design *A*. As the length of coil decreases, the resistance of coil will also decrease and the copper loss can be reduced to maintain the power from loss. I is current, R is the resistivity, t is the temperature, ρ is the material permittivity, L is the length of the wire and A is the area of the wire.

$$\text{Copper Loss} = I^2 \cdot R \cdot t \quad (2)$$

$$R = \rho \cdot \frac{L}{A} \quad (3)$$

Furthermore, the Maxwell coils pair arrangement also gives a positive impact on the magnetic field strength generated from the five vertically stacked coils between it as can be seen in Fig. 6. The magnetic field from the Maxwell coils pair, *B* will flow towards the five vertically stacked coils and will increase the total magnetic field strength generated by them to the targeted point of 10 mm - 50 mm.

Note that the Maxwell coils pair was used in this work to increase the induced magnetic field produced by the five vertically stacked coils instead to create the FFP as normally used by other MPI researchers. This suggests a new idea of the function of the Maxwell coils pair in MPI besides to create the FFP.

Table 4 - Magnetic field strength generated from the coils in Design *A* and Design *B* coil systems

Distance (mm)	Design *A* (μT)	Design *B* (μT)
10	1.8020	17.2835
20	1.1285	9.9190
30	0.6167	5.7624
40	0.2688	2.5674
50	0.0284	1.2230

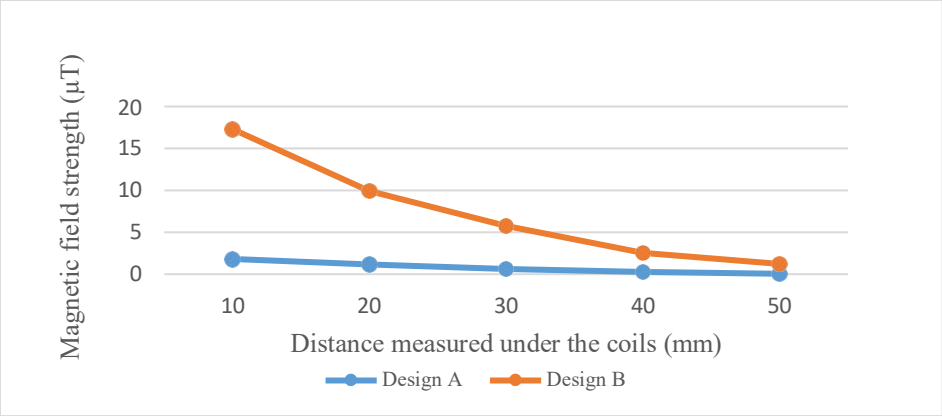

Fig. 5 - Magnetic field strength generated from the Design *A* and Design *B* coil systems when measured at different distances under the coil design

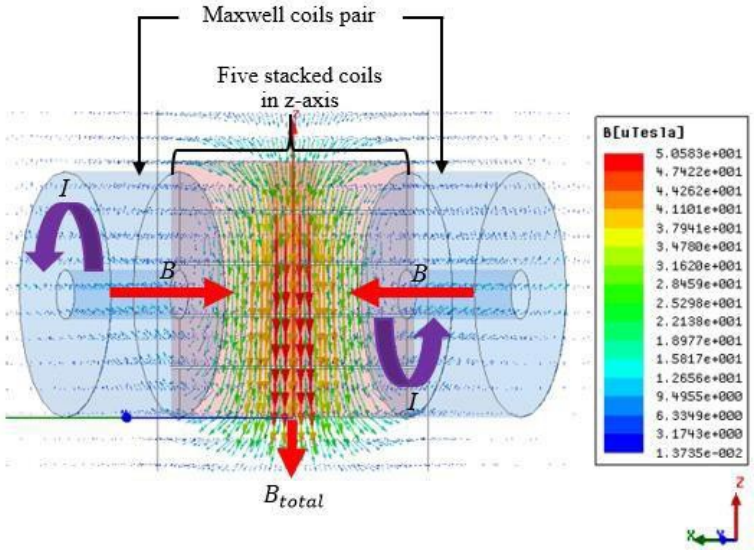

Fig. 6 - Magnetic field distribution from Design *B*. Magnetic field strength was indicated by the rainbow colour spectrum on the right top side of the figure

3.2 Magnetic Field Homogeneity Distributed from Both Coil Designs

Fig. 7 shows the homogeneity of the magnetic field distributed from both Design *A* and Design *B*, Fig. 7 (a) and Fig. 7 (b), respectively. From the simulation results, it can be seen that the magnetic field direction produced from the coils in Design *B* was more homogeneous than Design *A* towards the centre of the distribution area (yellow plane).

Different coils arrangement between the two designs affected the homogeneity of the magnetic field distribution. Coils arrangement in Design *B* were arranged with five vertically stacked coils placed between the Maxwell coils pair while in Design *A* six single coils that were arranged horizontally in the same plane. When the coils were arranged vertically in the same axis, the magnetic field direction generated from them will be aligned in the same direction and this can produce a more homogeneous magnetic field distribution than the coils that were arranged in the horizontal position.

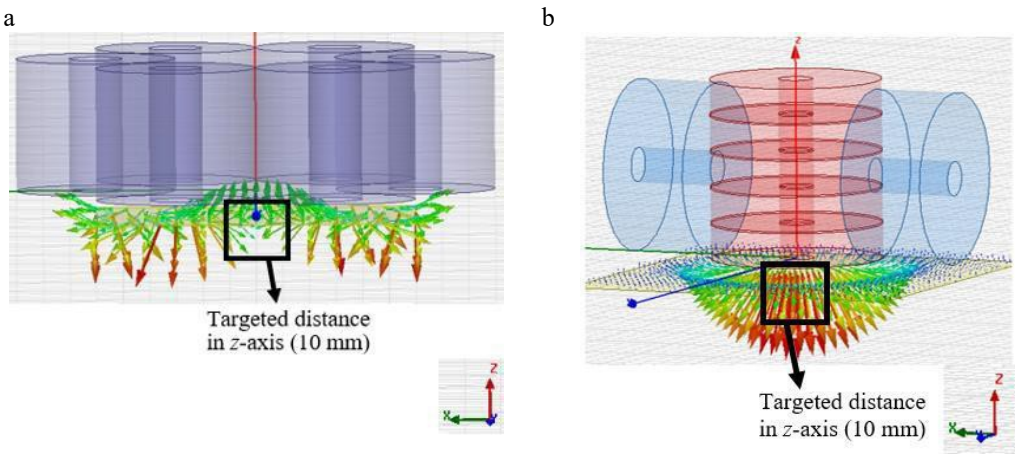

Fig. 7 - Magnetic field homogeneity distribution from the coil design at a distance of 10 mm (a) Design *A*; (b) Design *B*

3.3 Comparison between Simulation and Calculation Results of the Magnetic Field Strength Generated from Design *B* Coil System

The magnetic field strength generated by the coils in Design *B* obtained from the simulation was compared with the calculation that was evaluated by using equation (1). Fig. 8 shows the comparison between simulation and calculation results of the magnetic field strength generated from the coils by Design *B* at different positions in the z-axis. Magnetic field strength generated from both works shows the almost similar value for depth of 10 mm - 30 mm under the coils. For instance, when the magnetic field strength was determined at point 10 mm under the coils, the results for simulation and calculation were 16.7126 µT and 17.0516 µT, respectively. However, the magnetic field strength that was determined at point 40 mm - 50 mm showed slightly different values. For example, when the magnetic field strength was determined at point 50 mm under the coils, the results for simulation and calculation were 0.1966 µT and 3.0007 µT, respectively. The different value might be caused by the magnetic field strength generated by the Maxwell coils pair that not considered in the calculation work even if exist in the simulated model.

In addition, the calculated result shows a higher value of strength than the simulated result. The different values can be ignored as it is in the µT unit which is a very small range of unit scale. Therefore, the simulation data obtained from Design *B* was successfully proven and supported by the mathematical calculation as previously explained.

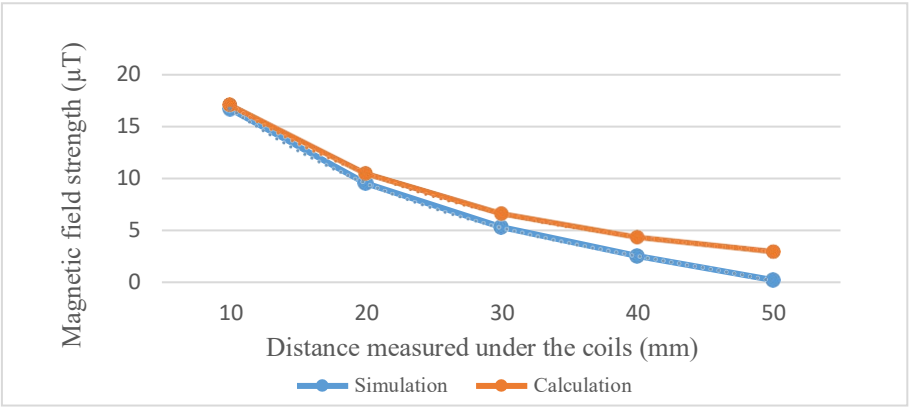

Fig. 8 - Comparison between simulation and calculation results of the magnetic field strength generated from the coils in Design *B* at different positions under the coils

4. Conclusion

This work presented two designs of an excitation coil system that were simulated by using ANSYS Maxwell to measure the magnetic field strength generated towards the MNPs located at a targeted distance 10 mm - 50 mm under the excitation coil. From the simulation data obtained, the Design *B* generated a stronger and more homogeneous magnetic field than those from Design *A*. Then, the simulated magnetic field strength from the coils in Design *B* was

compared to the mathematical calculation for validation. A good agreement was obtained between both simulated and calculated data for the Design *B* coil system. The improvement of magnetic field strength and its homogeneity can be obtained based on the combination of the stacked coils with a Maxwell coils pair. Therefore, a new concept of an excitation coil configuration system can be proposed from the findings and can be used for a single-sided MPI system for future development in a medical imaging application.

Acknowledgements

The authors would like to acknowledge the Geran Penyelidikan Pascasiswazah (GPPS) Vot H308, comstech-twas Joint research grant X071 and Universiti Tun Hussein Onn Malaysia (UTHM) for the support in this study.

References

[1] A. Weber, J. Weizenecker, J. Rahmer, J. Franke, U. Heinen, and T. Buzug, "Resolution improvement by decreasing the drive field amplitude," in *2015 5th International Workshop on Magnetic Particle Imaging (IWMPI)*, 2015, vol. 435, no. June, pp. 1-1.

[2] K. Shimada and K. Murase, "Effect of Signal Filtering on Image Quality of Projection-Based Magnetic Particle Imaging," *Open J. Med. Imaging*, vol. 7, no. 2, pp. 43-55, 2017.

[3] I. Khan, K. Saeed, and I. Khan, "Nanoparticles : Properties, applications and toxicities," *Arabian Journal of Chemistry*, Arabian Journal of Chemistry, 18-May-2017.

[4] S. Ilbey, C. B. Top, T. Cukur, E. U. Saritas, and H. E. Guven, "Image reconstruction for Magnetic Particle Imaging using an Augmented Lagrangian Method," in *Proceedings - International Symposium on Biomedical Imaging*, 2017, pp. 64-67.

[5] B. Gleich and J. Weizenecker, "Tomographic imaging using the nonlinear response of magnetic particles," *Nature*, vol. 435, no. 7046, pp. 1214-1217, 2005.

[6] T. Thiel, "Bruker Announces the World's First Preclinical Magnetic Particle Imaging (MPI) System," *Bruker Corporation*, 2013. [Online]. Available: https://ir.bruker.com/press-releases/press-release-details/2013/Bruker-Announces-the-Worlds-First-Preclinical-Magnetic-Particle-Imaging-MPI-System/default.aspx. [Accessed: 28-Jul-2019].

[7] J. Weizenecker, J. Borgert, and B. Gleich, "A simulation study on the resolution and sensitivity of magnetic particle imaging," *Phys. Med. Biol.*, vol. 52, no. 21, pp. 6363-6374, 2007.

[8] T. F. Sattel *et al.*, "Single-sided device for magnetic particle imaging," *J. Phys. D. Appl. Phys.*, vol. 42, no. 2, 2009.

[9] T. Knopp, T. F. Sattel, S. Biederer, and T. M. Buzug, "Field-free line formation in a magnetic field," *J. Phys. A Math. Theor.*, vol. 43, no. 1, pp. 1-9, 2010.

[10] T. Knopp *et al.*, "Model-Based Reconstruction for Magnetic Particle Imaging," *IEEE Trans. Med. Imaging*, vol. 29, no. 1, pp. 12-18, 2010.

[11] T. Knopp, S. Biederer, T. F. Sattel, M. Erbe, and T. M. Buzug, "Prediction of the Spatial Resolution of Magnetic Particle Imaging Using the Modulation Transfer Function of the Imaging Process," *IEEE Trans. Med. Imaging*, vol. 30, no. 6, pp. 1284-1292, 2011.

[12] P. Vogel *et al.*, "MRI Meets MPI : A Bimodal MPI-MRI Tomograph," *EEE Trans. Med. IMAGING*, vol. 33, no. 10, pp. 1954-1959, 2014.

[13] B. Zheng *et al.*, "Magnetic Particle Imaging tracks the long-term fate of in vivo neural cell implants with high image contrast," *Nat. Publ. Gr.*, vol. 5, no. 1, pp. 1-9, 2015.

[14] K. Gräfe, A. Von Gladiss, G. Bringout, M. Ahlborg, and T. M. Buzug, "2D Images Recorded With a Single-Sided Magnetic Particle Imaging Scanner," *IEEE Trans. Med. Imaging*, vol. 35, no. 4, pp. 1056-1065, 2016.

[15] A. Ohki, M. Tanoue, and S. Kobayashi, "Magnetic Particle Imaging for Quantitative Evaluation of Tumor Response to Magnetic Hyperthermia Treatment Combined with Chemotherapy Using Cisplatin," *Therm. Med*, vol. 33, no. 2, pp. 39-51, 2017.

[16] Y. Muslu, M. Utkur, O. B. Demirel, and E. U. Saritas, "Calibration-Free relaxation-based multi-color magnetic particle imaging," *IEEE Trans. Med. Imaging*, vol. 37, no. 8, pp. 1920-1931, 2018.

[17] O. Kosch *et al.*, "Evaluation of a separate-receive coil by magnetic particle imaging of a solid phantom," *J. Magn. Magn. Mater.*, vol. 471, pp. 444-449, 2019.

[18] H. J. Ann, L. S. Su-Shi, and Z. Zakaria, "Non-invasive breast cancer assessment using magnetic induction spectroscopy technique," *Int. J. Integr. Eng.*, vol. 9, no. 2, pp. 54-60, 2017.

[19] T. M. Buzug, "Magnetic Particle Imaging - from particle science to imaging technology," *Biomed. Tech. Eng.*, vol. 58, no. 6, 2013.

[20] G. Bringout and T. M. Buzug, "Coil Design for Magnetic Particle Imaging: Application for a Preclinical Scanner," *IEEE Trans. Magn.*, vol. 51, no. 2, pp. 1-8, 2015.

[21] H. Wojtczyk *et al.*, "Toward the Optimization of D-Shaped Coils for the Use in an Open Magnetic Particle Imaging Scanner," *IEEE Trans. Magn.*, vol. 50, no. 7, pp. 1-7, 2014.

[22] G. Bringout *et al.*, "High power driving and selection field coil for an open MPI scanner," in *2013 International Workshop on Magnetic Particle Imaging, IWMPI 2013*, 2013.

[23] N. B. Othman, T. Tsubaki, T. Yoshida, K. Enpuku, and A. Kandori, "Magnetic Nanoparticle Imaging Using Harmonic Signals," *IEEE Trans. Magn.*, vol. 48, no. 11, pp. 3776-3779, 2012.

[24] T. Le and A. K. Hoshiar, "A Soft Magnetic Core can Enhance Navigation Performance of Magnetic Nanoparticles in," *IEEE/ASME Trans. Mechatronics*, vol. 23, no. 4, pp. 1573-1584, 2018.

[25] A. Yadav, "Effect of Temperature on Electric Current, Magnets and Electromagnet," *Int. J. Adv. Technol.*, vol. 07, no. 04, 2016.

[26] S. Abdulkareem, A. A. Khan, Q. Shah, and M. Konneh, "Temperature distribution in copper electrode during electrical discharge machining process," *Int. J. Integr. Eng.*, vol. 9, no. 1, pp. 39-43, 2017.

[27] M. Fadhzir *et al.*, "Effect of Temperature and Current Density on Polybenzimidazole Zirconium Phosphate Hybrid Membrane in Copper Chloride Electrolysis for Hydrogen Production," *Int. J. Integr. Eng.*, vol. 11, no. 7, pp. 182-189, 2019.

[28] D. Lin and E. F. Fuchs, "Real-time monitoring of iron-core and copper losses of transformers under (non)sinusoidal operation," *IEEE Trans. Power Deliv.*, vol. 21, no. 3, pp. 1333-1341, 2006.

[29] Y. C. Cho *et al.*, "Copper Better than Silver: Electrical Resistivity of the Grain-Free Single-Crystal Copper Wire," *Cryst. Growth Des.*, vol. 10, no. 6, pp. 2780-2784, 2010.